Particle response and turbulence modification in isotropic turbulence

Kyle D. Squires and John K. Eaton
Department of Mechanical Engineering, Stanford University, Stanford, California 94305

(Received 28 December 1989; accepted 26 March 1990)

The effect of turbulence on particle concentration fields and the modification of turbulence by particles has been investigated using direct numerical simulations of isotropic turbulence. The particle motion was computed using Stokes' law of resistance and it was also assumed the particle volume fraction was negligible. For simulations in which the particles do not modify the turbulence field it was found that light particles collect preferentially in regions of low vorticity and high strain rate. For increased mass loading the particle field attenuated an increasing fraction of the turbulence energy. Examination of the spatial energy spectra showed that the fraction of turbulence kinetic energy in the high wave numbers was increased relative to the energy in the low wave numbers for increasing values of the mass loading. It was also found that the turbulence field was modified differently by light particles than by heavy particles because of the preferential collection of the light particles in low-vorticity, high-strain-rate regions. Correlation coefficients between the second invariant of the deformation tensor and pressure showed little sensitivity to increased loading while correlations between enstrophy and pressure were decreased more by the light particles than by the heavy particles for increased mass loading.

I. INTRODUCTION

A. General

The motion of heavy particles through a turbulent flow field provides one of the most interesting research topics in fluid mechanics. Aside from requiring knowledge of the statistical properties of the turbulence, the dynamics and kinematics of particle motion must also be known in order to close the problem. This is made somewhat more complicated by particles that cannot follow all the fluctuations of the turbulent velocity field. Prediction of turbulent flows laden with heavy particles is of practical engineering interest since these flows occur in many technologically important areas, flows in energy conversion devices or problems in pollution control being two examples.

Two of the most important problems arising when particles are introduced into a turbulent flow are the dispersion of particles by turbulence and modification of turbulence properties by particles. Problems of particle dispersion by turbulence are usually studied, assuming that the properties of the turbulent flow field are not modified by the presence of the particle cloud (i.e., "one-way coupling"[1]). Problems of turbulent dispersion of particles have shown to be more suitably analyzed using a Lagrangian reference frame.[2,3] This is precisely the difficulty in studying problems of turbulent diffusion experimentally since it is typically not straightforward to acquire statistical information following particle trajectories in the laboratory. The experiments by Snyder and Lumley[4] and Wells and Stock[5] in grid-generated turbulent flows have provided some useful information concerning the problem of turbulent dispersion of particles. Numerical simulations have also provided a means of acquiring Lagrangian statistical data of both fluid elements and heavy particles in turbulent flows (e.g., Elghobashi and Truesdell,[6] Fung and Perkins,[7] McLaughlin,[8] Squires and Eaton,[9,10] and Yeung and Pope[11]). Since the primary topic of this paper is turbulence modification by particles the reader is referred to Squires and Eaton[9,10] for a more complete review of the problem of particle dispersion by turbulence.

Problems of turbulence modification by particles arise when particles are present in large enough concentrations such that the momentum loss or gain to the turbulence provided by the particles is no longer negligible (i.e., "two-way coupling"[1]). Conventional wisdom implies that the presence of particles provides an additional dissipation or attenuation of turbulence. However, it is not clear how this extra dissipation may be incorporated into turbulence models or how it depends on the parameters of the problem, such as the particle time constant, mass loading (i.e., ratio of the particle mass to that of the carrier fluid), and the various dimensionless parameters describing the turbulence. It would seem quite possible that particles selectively concentrated in particular structures may cause rapid attenuation of that structure or trigger a new instability mechanism. Thus it is important to determine the effect of the turbulence structure on the behavior of the particle cloud.

B. Influence of turbulence on particle motions

Traditional statistical approaches for examining the influence of turbulence on particle motions may not be appropriate for some applications. For example, in reacting flows knowledge of the instantaneous particle concentration field is required and therefore it is important to understand the influence of the turbulence structure on particle motions and resulting particle concentration fields. This information is also critical for problems of turbulence modification by particles since significant effects of turbulence on particle concentration fields will subsequently influence how the turbulence is modified.

 0899-8213/90/071191-13$02.00

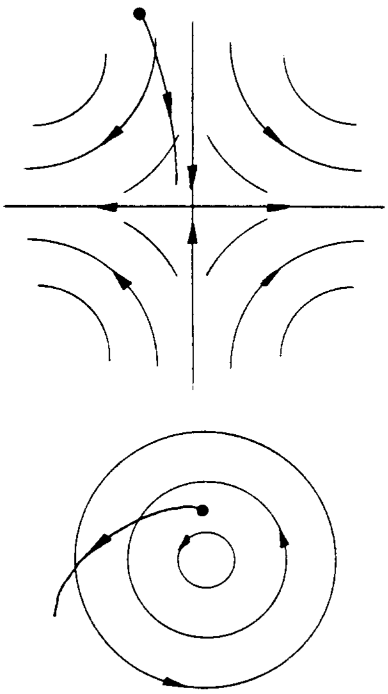

FIG. 1. Particle motion in the vortex and strain fields.

Recent experiments have shown that turbulence structures can significantly influence the particle concentration field. Measurements of particle dispersion in the plane mixing layer have been obtained by Kobayashi *et al.*,[12] Kamalu *et al.*,[13] and Lazaro and Lasheras.[14] Longmire and Eaton[15] have examined particle dispersion in round jets. These investigators have obtained instantaneous measurements of the particle concentration field and find it is strongly correlated with the large vortex structure of the free shear layer. For example, in the experiments of Longmire and Eaton it has been found that a round jet collects particles into the saddle region between successive vortex rings.

Computational studies have also been useful in examining the effect of turbulence on particle concentration fields. This work includes Maxey's[16] examination of gravitational settling of aerosol particles in velocity fields comprised of random Fourier modes. By treating the particles as a compressible flow field he showed that particles will tend to accumulate in regions of low vorticity and high strain rate. Figure 1 shows a simple schematic of a particle in a plane vortex and pure straining flow. Because of the particle's inertia it cannot follow the streamlines of the vortex and will tend to drift away from the vortex center, whereas for the pure straining flow the particle will drift toward the stagnation point. Fung and Perkins[7] have also examined particle motions in flow fields composed of random Fourier modes and find that for certain ratios of the particle time constant to characteristic fluid time scale there is a "trapping" of particles within eddies. Chein and Chung[17] have performed simulations of the mixing layer using a vortex method and have shown that particles may be dispersed more than fluid elements because of a "flinging" effect of the large-scale vortex structures. Squires and Eaton[18] examined particle response in direct numerical simulations of isotropic turbulence and found that the number density of light particles was as much as 40 times the mean value in low-vorticity, high-strain-rate regions.

C. Turbulence modification by particles

Turbulence modification by particles occurs when the particles are present in sufficiently large concentrations such that the momentum loss or gain to the turbulence by the particle cloud is no longer negligible. This subset of particle-laden flows has not been investigated as thoroughly as that of particle dispersion by turbulence, primarily because of the difficulty in obtaining reliable laboratory measurements. Computations of turbulence modification by particles are also limited in their usefulness because of the lack of reliable turbulence models.

Laboratory measurements of turbulence modification by particles are difficult to obtain in the presence of a large concentration of dispersed particles. Often, changes in the mean flow caused by the particles cause changes in the turbulence properties, masking effects of the particle cloud on the turbulence. Other effects such as nonuniform particle size, mass loading, flow Reynolds number, and particle diameter can have a significant impact on the results from laboratory experiments. Gore and Crowe[19] reviewed studies of turbulence modification in pipe and jet flows. The key parameter of their analysis is the ratio of the particle diameter to a characteristic length scale of the turbulence. For small values of this parameter they found the turbulence to be attenuated by the dispersed phase while the turbulence is amplified for large values.

Experimental effort in turbulence modification include the Lee and Durst[20] examination of turbulence modification by particles in a turbulent pipe flow. In this experiment it was found that smaller particles damped the turbulent fluctuations. Arnason and Stock[21] also examined turbulence modification in a pipe flow and noted increased turbulence levels when particles were added to the flow. Tsuji and Morikawa[22] examined turbulence modification in a horizontal pipe. Nonuniform particle loading induced by gravitational settling caused distortions in the mean velocity profile. In this experiment it was found that turbulence levels were increased by large particles and decreased by small particles. Rogers and Eaton[23] have performed a series of experiments on turbulence modification in a two-dimensional boundary layer. A uniform loading of particles prevented changes from occurring in the mean velocity profile. It was found that the presence of the particles decreased the turbulence intensity as much as 20% for mass loadings up to 0.2

Computational approaches to the problem of turbulence modification by particles include the work by Tang *et al.*,[24] who examined turbulence modification by particles in the plane mixing layer using a vortex method. In these simulations the particles inhibited the development of the initial instability forming large-scale vortices but did not affect subsequent pairing of the vortex structures or the growth of the mixing layer. Squires and Eaton[18] investigated turbulence modification by particles using direct numerical simulation of forced isotropic turbulence and found the frequency spectrum of the turbulence to be uniformly attenuated by the presence of the particles.

D. Objectives

Previous experiments and computations have provided some useful information concerning the influence of turbulence on the behavior of the particle concentration field as well as turbulence modification by particles. In order to improve predictive capabilities of particle-laden turbulent flows more detailed information is required regarding the influence of turbulence structure on particle behavior and turbulence modification by particles. One approach to acquiring this information is through the use of direct numerical simulation (DNS) in which the Navier–Stokes equations are solved without resorting to turbulence modeling. Results obtained from direct numerical simulation provide detailed three-dimensional, time-dependent information at a large number of grid points. It is also relatively straightforward to follow the trajectories of particles through the flow fields generated by DNS using suitable interpolation techniques. DNS is limited to low Reynolds numbers but can yield significant advances when information is needed that cannot be obtained from experiment.

In order to increase the basic understanding of the influence of turbulence on particle behavior, as well as the problem of turbulence modification by particles, direct numerical simulation of forced isotropic turbulence with particles was performed. The research addressed the simplest type of flow: homogeneous, isotropic turbulence and examined interactions between the particles and turbulence. The specific range of problems examined include those in which the particle is much smaller than the smallest length scales of the turbulence yet heavy enough to slip relative to the flow. The particle mass loading is large enough to have a significant impact on the turbulence while the volume fraction of particles was small enough such that particle–particle interactions could be neglected. This situation, large mass loading with negligible volume loading, occurs commonly when solid particles are conveyed by gas flow. The results presented in this paper include quantities such as time histories of the turbulence energy, spatial energy, and dissipation spectra as well as "structural" measures of the turbulence, quantities such as conditional expectations of the number density, enstrophy, and second invariant of the deformation tensor. This work extends the earlier results obtained by Squires and Eaton[18] by using finer resolution of the turbulence field for the hydrodynamic computation as well as a larger statistical sample of particles.

II. BACKGROUND

A. Governing equations

The equation of motion for a sphere in a turbulent flow field is a complicated integrodifferential equation (e.g., see Maxey and Riley[25]). However, for many applications the equation of motion may be greatly simplified. For example, if the density of the particle is much greater than the density of the carrier fluid (e.g., solid particles in air) then many of the forces in the equation of motion are negligible compared to the drag force. Furthermore, if the drag force obeys Stokes' law then the equation of motion is linear in the velocity difference between fluid and particle. The equation of particle motion integrated in the present simulations was

$$\frac{dv_i}{dt}=\alpha\{u_i[X_{pi}(t),t]-v_i(t)\},\tag{1}$$

where $X_{pi}(t)$ and $v_i(t)$ are the position and velocity of the particle. The coefficient α is the inverse of the particle response time and for the linear drag law used in (1) is given by

$$\alpha=18\mu/\rho_p d^2.\tag{2}$$

In (2), μ is the dynamic viscosity of the carrier fluid, ρ_p is the particle density, and d is the particle diameter. Equation (1) represents a balance of the particle acceleration with the drag force. For α, as given by Eq. (2), the drag force in (1) is assumed to obey Stokes' law. This is appropriate if the Reynolds number based on the relative velocity between the particle and fluid is significantly less than unity. The particle is also assumed to be smaller than the smallest length scales of the fluid flow field. For a turbulent flow this means that the particle diameter is smaller than the Kolmogorov scale η.[25] It is also assumed that particle–particle interactions are negligible. Since the primary objective of this paper is to study the effects of turbulence on particle motion and turbulence modification by particles the effect of an external body force is neglected. For studies of particle dispersion by turbulence the effect of an external body force significantly alters the dispersion characteristics of the particles (e.g., see Elghobashi and Truesell[6] and Squires and Eaton[10]).

The fluid continuity equation is unchanged by the presence of the particles since the volume fraction of the particles is negligible. The effect of particles on turbulence appears as an additional force in the momentum equation of the fluid. For an incompressible fluid the equations of motion for the carrier fluid are then

$$\frac{\partial u_i}{\partial x_i}=0,\tag{3}$$

$$\frac{\partial u_i}{\partial t}+\frac{\partial u_i u_j}{\partial x_j}=\frac{-1}{\rho}\frac{\partial P}{\partial x_i}+\nu\frac{\partial^2 u_i}{\partial x_j\,\partial x_j}-\frac{\alpha c}{\rho}(u_i-v_i)\tag{4}$$

(throughout this paper repeated indices imply summation). In Eq. (4), c is the particle "concentration," i.e., mass of particles per unit volume.

B. Overview of the simulations

The numerical method used in the present research is based on the pseudospectral technique developed by Rogallo.[26] In this method the incompressible Navier–Stokes equations are solved by expanding the velocity field in a Fourier series,

$$u_j(\mathbf{x},t)=\sum_{\mathbf{k}} \hat{u}_j(\mathbf{k},t)\exp i\mathbf{k}\cdot\mathbf{x}, \tag{5}$$

and then using the orthogonality property of $\exp i\mathbf{k}\cdot\mathbf{x}$ to obtain equations for the Fourier coefficients $\hat{u}_j(\mathbf{k},t)$. Expanding the velocity field in a Fourier series allows for extremely accurate evaluation of spatial derivatives.[27] In a pseudospectral method evaluation of the nonlinear terms gives rise to aliasing errors that are eliminated using a combination of phase shifts and truncation. The time advance scheme is second-order Runge–Kutta. For more details of the method see Rogallo[26] and Lee and Reynolds.[28]

The particle momentum equation was time advanced using the same scheme as for the hydrodynamic calculation, a second-order Runge–Kutta scheme. At each substep the fluid velocity at the particle position was interpolated using vectorized trilinear interpolation. More accurate interpolation schemes would, of course, increase the accuracy of the interpolated velocities but at an increased computational cost. The results presented in this paper were obtained by following the trajectories of as many as 10^6 particles and the simulations required as much as 20 h of CPU time on a Cray-2 supercomputer. Thus it was necessary to use an inexpensive interpolation scheme.

The incorporation of the effect of the particles on the turbulence is based on the particle-source-in-cell (PSIC) method of Crowe[1] using Eq. (4). The implementation of the PSIC scheme for these simulations differed from Crowe's in that the source term calculated for each particle was interpolated back to the eight grid points surrounding the particle using volume-weighted averages. Unfortunately, calculation of the source term is not a vector operation and is the most expensive part of a single time step. Computation of the source term per time step for 10^6 particles required approximately 45 CPU seconds using a Cray-2 (for the second-order Runge–Kutta scheme).

The problem studied is homogeneous, isotropic turbulence. "Natural" isotropic turbulence decays and the lack of stationarity complicates analysis of the results. Thus stationary isotropic turbulence was obtained by artificially forcing the low wave numbers (large scales) at each time step. The forcing scheme used for these simulations was identical to that of Hunt *et al.*[29] In this method a steady, nonuniform force field is introduced at the largest scales of the flow. The forcing coefficients are constrained to satisfy the continuity condition as well as isotropy of the velocity field. Results presented in this paper were obtained from simulations using 32^3 and 64^3 points for the hydrodynamic computation and tracking 3.73×10^5 or 10^6 particles. The ratio of the time constant to the fluid time scale defined using the longitudinal integral length scale and $(q^2/3)^{1/2}$ was varied from 0.075 to 1.50 and the mass loading was varied from 0.1 to 1.0. The parameters of the particles and mass loadings used in the simulations are summarized in Table I. Simulations using all mass loadings were performed for each particle time constant except for $\tau_p/\tau_e=0.075$.

For each simulation the two phases were uncoupled and time advanced to reach a statistically stationary state and eliminate initial transients of the forcing. When a statistically stationary state had been reached the momentum equation of the fluid was coupled to the particle momentum equation with a specified mass loading. Once the phases were coupled the 32^3 simulations were time advanced slightly over 12 eddy turnover times while the 64^3 simulations were advanced approximately six eddy turnover times. The eddy turnover time τ_Λ is defined as

TABLE I. Simulation parameters.

ϕ	τ_p/τ_e	Grid size
0.1	0.14	32^3
0.5	0.75	32^3
1.0	1.50	32^3
	0.075	64^3
	0.15	64^3
	0.52	64^3

$$\tau_\Lambda=\Lambda/q, \tag{6}$$

where Λ is the integral scale of the turbulence, defined as

$$\Lambda=\frac{3\pi}{2q^2}\int_0^\infty \frac{E(k)}{k}\,dk \tag{7}$$

and q^2 is twice the turbulence kinetic energy.

Sampling the time series every ten time steps was found to adequately resolve the highest frequencies of the flow. At every sampling interval the particle position and velocity and fluid velocity at the particle position were stored for later post-processing. The time histories of 2000 particles were used to compute power spectra and other time series statistics. Statistics of the number density of particles were computed by subdividing the flow field into cells, each cell surrounding one grid point. Within each cell particle properties were then defined by averaging over the particles contained in the cell.

Results from the simulations of no coupling ($\phi=0$, where ϕ is the mass loading) between the phases provide a baseline case to compare the effect of increased mass loading on turbulence statistics. These simulations are also useful for examining the effect of turbulence "structure" on the particle concentration field. For these baseline simulations the Reynolds number based on the Taylor microscale and twice the turbulence kinetic energy was approximately 37 for the 32^3 simulations and 38 for the 64^3 simulations. Simulations using these Reynolds numbers assured good resolution of the velocity field. One measure of small-scale resolution is the parameter $k_{\max}\eta$, where $k_{\max}$ is the maximum wave number of the computation and η is the Kolmogorov length scale. The maximum wave number is determined by the dealiasing scheme and for Rogallo's code $k_{\max}=\sqrt{2}N/3$, where N is the number of points in one direction. A value of $k_{\max}\eta$ greater than 1.0 provides adequate resolution of low-order statistics[11] and for the baseline simulations the value of this parameter was 1.65 for the 32^3 simulations and 1.41 for the 64^3 simulations.

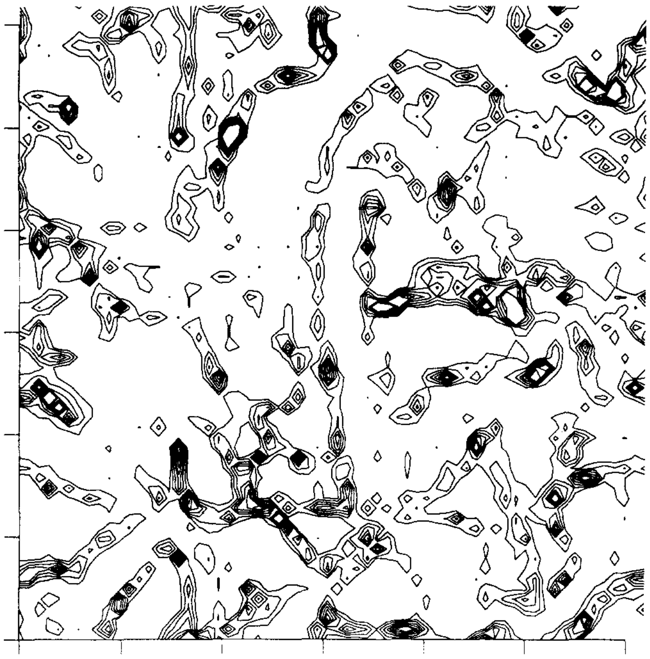

(a)

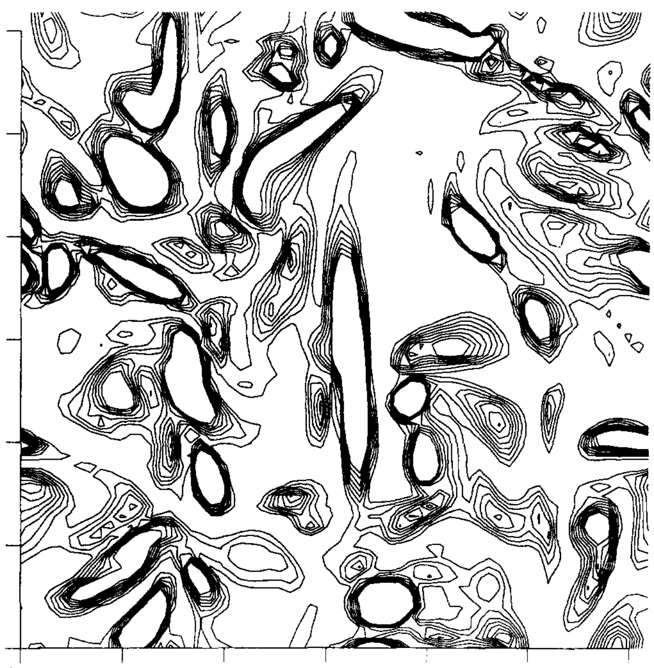

(b)

FIG. 2. (a) Number density contours from the 64^3 simulation, $\tau_p/\tau_e = 0.15$, contour levels between $\bar{n}$ and $7\bar{n}$ (b) enstrophy contours from the 64^3 simulation, contour levels between $0.5\bar{\varepsilon}$ and $2.25\bar{\varepsilon}$.

III. RESULTS

A. Structure of the number density field

Contours of the particle number density for $\tau_p/\tau_e = 0.15$ and $\phi = 0$ are shown in Fig. 2(a). The contours shown are taken from one plane of the 64^3 computations. Enstrophy contours in this plane are shown in Fig. 2(b). It is evident from Fig. 2(a) that the particles are not uniformly dispersed throughout the volume and there are distinct regions of particle accumulation. The peak number density in this plane is approximately 30 times the mean value. By comparing Fig. 2(a) with the enstrophy contours in Fig. 2(b) it is apparent that the regions of high particle concentration are associated with regions of low vorticity.

Figures 3(a) and 3(b) are the contours of the number density for $\tau_p/\tau_e = 0.15$ and $\tau_p/\tau_e = 0.52$ from the 64^3 simulations, again for the case $\phi = 0$. In these figures only a portion of the plane from Fig. 2 has been shown. Contours of the enstrophy in this portion of the plane are shown in Fig. 3(c). Comparison of Figs. 3(a) and 3(b) with Fig. 3(c) show that as the particles become more sluggish (i.e., larger time constants) the tendency to accumulate in regions of low vorticity is decreased. It was found that the lightest particles used for the 64^3 simulations, $\tau_p/\tau_e = 0.075$, showed a *decreasing* tendency to collect in regions of low vorticity. This is consistent with the idea that very light particles behave more as fluid elements and therefore show no tendency to collect in these regions. Thus the behavior of extremely light and extremely heavy particles is similar in the sense that neither will show a tendency to collect in low-vorticity regions. It is important to keep in mind, therefore, that an optimum ratio of the particle time constant to a fluid time scale exists such that particles will show this preferential concentration.

Examination of the conditional expectations of the number density assist in quantifying the effect of the preferential concentration of particles. The conditional expectation of the number density, given the magnitude of vorticity, is shown in Fig. 4 for each of the particle time constants used in the 64^3 simulations (for $\phi = 0$). This figure clearly shows that for small values of the vorticity the number density of particles is increased over the mean value and that in regions of high vorticity the number density of particles is small. It may also be seen from the figure that the lightest particles used in the 64^3 simulations, $\tau_p/\tau_e = 0.075$, show less of a tendency to be in regions of low vorticity than do particles with the dimensionless time constant of 0.15.

Maxey[16] has shown that heavy particles will tend to collect in regions of high strain rate as well as regions of low vorticity. This effect can be quantified by using the second invariant of the deformation tensor, $\partial u_i/\partial x_j$. The second invariant of the deformation tensor is defined through the relation

$$-2II_d \equiv \frac{\partial u_i}{\partial x_j}\frac{\partial u_j}{\partial x_i}. \tag{8}$$

Regions where II_d is large and positive are regions of high vorticity and correspond to low values of the number density while regions of large negative II_d are regions of high strain rate and correspond to high values of the number density.

By expressing Eq. (8) in terms of the strain rate tensor and rotation tensor it may be shown that large values of

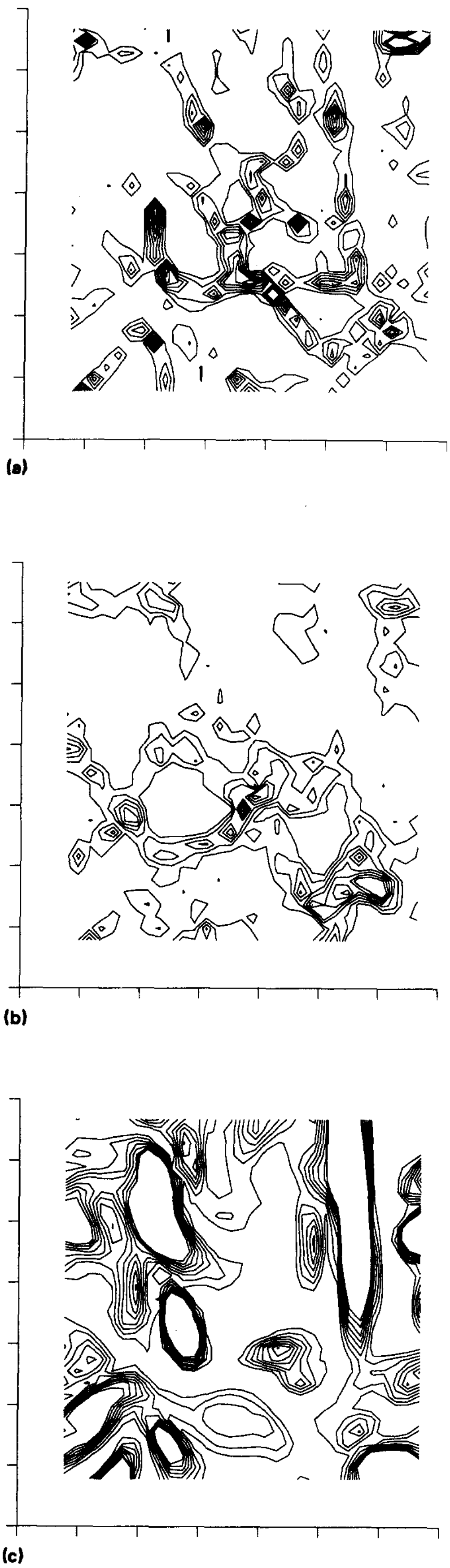

FIG. 3. Number density contours from 64^3 simulations, contour levels are the same as in Fig. 2(a). (a) $\tau_p/\tau_e = 0.15$; (b) $\tau_p/\tau_e = 0.52$ (c) enstrophy contours from the 64^3 simulation; the contour levels are the same as in Fig. 2(b).

II_d (positive and negative) represent regions of high vorticity or high strain. Using the definitions of the strain rate and rotation tensors, Eq. (8) may be expressed as

$$-2II_d = (S_{ij} + \Omega_{ij})(S_{ji} + \Omega_{ji}), \tag{9}$$

since

$$S_{ij} \equiv \frac{1}{2}\left(\frac{\partial u_i}{\partial x_j} + \frac{\partial u_j}{\partial x_i}\right) \tag{10}$$

and

$$\Omega_{ij} \equiv \frac{1}{2}\left(\frac{\partial u_i}{\partial x_j} - \frac{\partial u_j}{\partial x_i}\right). \tag{11}$$

Simplifying (9) gives

$$-2II_d = S_{ij}S_{ji} + \Omega_{ij}\Omega_{ji} + S_{ij}\Omega_{ji} + S_{ji}\Omega_{ij}. \tag{12}$$

Since S_{ij} is a symmetric tensor and Ω_{ij} is antisymmetric the last two terms on the right-hand side of (12) cancel and this equation may be rewritten as

$$-2II_d = S_{ij}S_{ji} - \Omega_{ij}\Omega_{ij}. \tag{13}$$

Substituting for Ω_{ij} in terms of the vorticity yields

$$II_d = (-1/2)(S^2 - \tfrac{1}{4}\omega_j\omega_j), \tag{14}$$

where S^2 is the magnitude of the strain rate tensor and ω_j is the jth component of vorticity.

The conditional expectation of the number density given by II_d is shown in Fig. 5 and illustrates the same features as those shown in Fig. 4, i.e., the number density of particles is less than the mean value in regions of high vorticity (large positive II_d). It may also be seen from Fig. 5 that the number density is as much as twice the mean in regions of high strain rate (large negative II_d). As could be seen from Fig. 4, particles with $\tau_p/\tau_e = 0.075$ show less tendency to collect in low-vorticity, high-strain rate regions than do particles with $\tau_p/\tau_e = 0.15$.

Correlation coefficients between number density and enstrophy as well as number density and II_d are contained in Table II for the 32^3 and 64^3 simulations. As can be seen from the table, the correlation between number density and enstrophy or II_d decreases for increasing particle inertia. The correlation of the number density and enstrophy is less than that between number density and II_d since this correlation measures the tendency for particles to be in regions of low vorticity *and* high strain rate.

B. Frequency spectra for $\phi = 0$

Frequency spectra from the 64^3 simulations are shown in Fig. 6 for $\phi = 0$. The fluid spectra plotted in this figure is the spectrum of the turbulent fluctuations along the particle path. For increasing particle inertia the energy at a given frequency is decreased over that of the fluid. The slight differences between the spectra of the fluid velocities for each of the time constants shown in Fig. 6 can be attributed to the sampling bias caused by lighter particles collecting in regions of low vorticity and high strain rate more than the heavier particles.

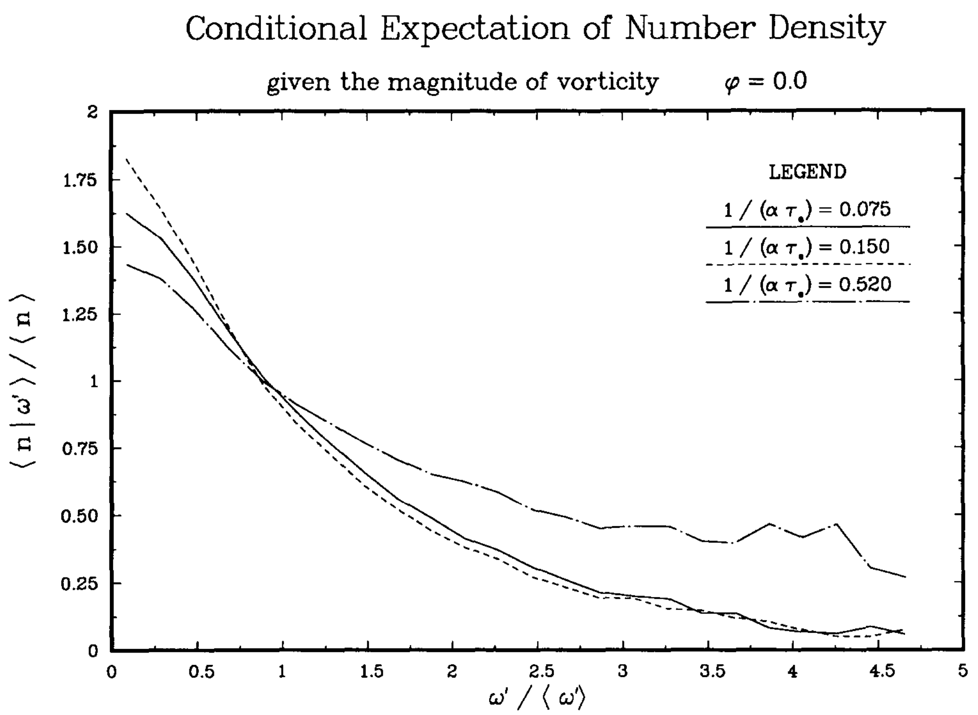

FIG. 4. Conditional expectation of the number density given vorticity magnitude from 64^3 simulations, $\phi = 0$.

The spectra of the particle velocities shown in Fig. 6 can be related to the spectra of the fluid velocities by using the particle equation of motion. This relationship takes the form

$$E_p(\omega) = E_f(\omega)/\eta(\omega), \tag{15}$$

where $\eta(\omega)$ is known as the response function. The specific form of $\eta(\omega)$ is dependent on the particle equation of motion (e.g., see Hinze[30]). For Stokes' law of resistance Eq. (15) is

$$E_p(\omega) = E_f(\omega)/(1 + \tau_p^2\omega^2). \tag{16}$$

It was found that agreement between the measured spectra of the particle velocities and the prediction of Eq. (16) was excellent for all values of the particle time constant or mass loading.

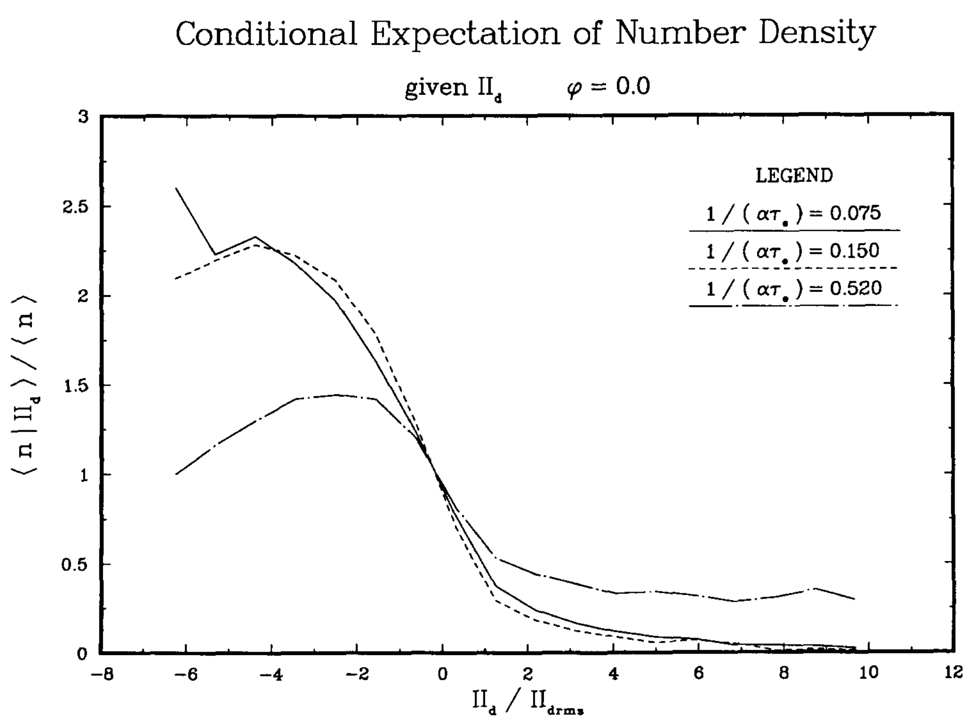

FIG. 5. Conditional expectation of the number density given the second invariant of the deformation tensor from 64^3 simulations, $\phi = 0$.

TABLE II. Correlation coefficients between number density and enstrophy $\overline{nce}$ and number density and II_d, $\overline{ncII_d}$, for $\phi = 0$.

τ_p/τ_e	$\overline{nce}$	$\overline{ncII_d}$
0.15	− 0.183	− 0.249
0.52	− 0.148	− 0.200
0.14	− 0.168	− 0.240
0.75	− 0.143	− 0.219
1.50	− 0.113	− 0.151

TABLE III. Turbulence energy and dissipation rate from 64^3 simulations.

ϕ	$\tau_p/\tau_e = 0.15$		$\tau_p/\tau_e = 0.52$	
	$q^2/q^2_{\phi=0}$	$\epsilon/\epsilon_{\phi=0}$	$q^2/q^2_{\phi=0}$	$\epsilon/\epsilon_{\phi=0}$
0.0	1.000	1.000	1.000	1.000
0.1	0.905	0.892	0.907	0.856
0.5	0.687	0.720	0.695	0.608
1.0	0.530	0.595	0.554	0.485

C. Effect of loading on turbulence energy and dissipation

For simulations performed using a nonzero mass loading an adjustment period was required to reach a new equilibrium after the particles and turbulence were coupled. This adjustment period was found to be between two and three eddy turnover times and increased for larger mass loadings. Time-averaged values of twice the turbulence kinetic energy q^2 and homogeneous dissipation ϵ from the 64^3 simulations are shown in Table III. The values shown in Table III correspond to the "steady-state" portion of the simulation, i.e., independent of the adjustment period that occurs after the beginning of coupling between the phases. It can be seen from Table III that the effect of increased mass loading is to decrease the turbulence energy and dissipation rate by as much as a factor of 2. For a mass loading of 1.0 and the heavier particles, the viscous dissipation is less than one-half the unloaded value. The total dissipation is constant for all cases so at a mass loading of 1.0 approximately one-half the total dissipation is due to particle drag. There is significant attenuation of the turbulence energy even at the lowest mass loadings (0.1), in agreement with the findings of Rogers and Eaton.[23]

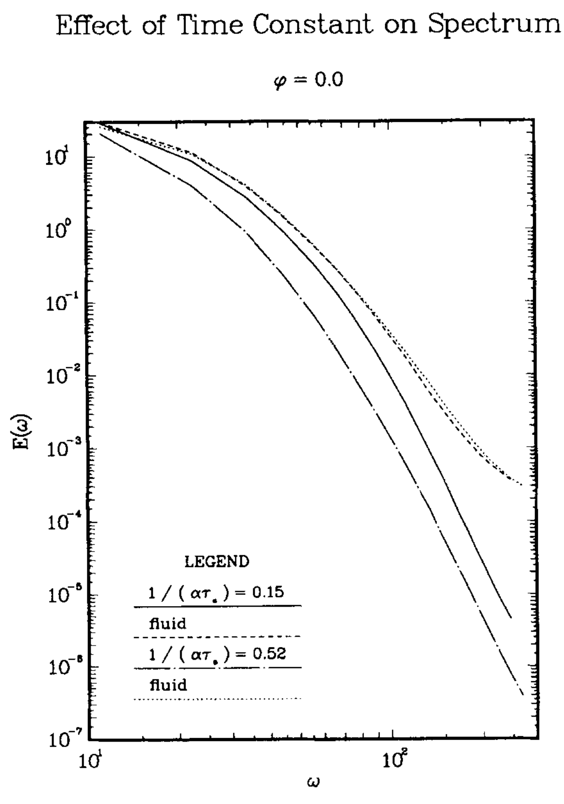

FIG. 6. Frequency spectra from 64^3 simulations, $\phi = 0$.

For the heavier particles used in the simulations, e.g., $\tau_p/\tau_e = 0.52$, the decrease of q^2 and ϵ from the beginning of coupling of the phases to the new equilibrium state was monotonic for all mass loadings. However, for $\tau_p/\tau_e = 0.15$ the dissipation initially increased from its $\phi = 0$ value before decreasing to the "steady-state" value shown in Table III for $\phi = 0.5$ and $\phi = 1.0$. This anomalous behavior is an artifact of the initial conditions from the simulations performed using nonzero mass loading. These simulations used as initial conditions the velocity and number density fields from the $\phi = 0$ simulations. It has been shown in Sec. III A that the lightest particles showed a pronounced tendency to collect in regions of low vorticity and high strain rate. This preferential particle concentration causes an initial increase in the dissipation that is not seen in the dissipation history for $\tau_p/\tau_e = 0.52$.

Examination of the transport equation for q^2 shows that the effect of the additional source term in the momentum equations of the fluid [Eq. (4)] arising from the particle coupling acts as a sink for the turbulence kinetic energy. The transport equation for q^2 for isotropic turbulence takes the form

$$\frac{dq^2/2}{dt} = P - \epsilon - \overline{c}\,(\overline{u_i'u_i'} - \overline{u_i'v_i'}) - (\overline{c'u_i'u_i'} - \overline{c'u_i'v_i'}), \quad (17)$$

where P is the turbulence production term and ϵ is the viscous dissipation and they are identical to the production and dissipation terms in a single-phase flow. From Eq. (17) it can be seen that the turbulence kinetic energy will be decreased by the presence of the dispersed phase if $\overline{u_i'u_i'}$ is greater than $\overline{v_i'v_i'}$. Since $\overline{v_i'v_i'}$ is a correlation of the fluid and particle velocities, it cannot be greater than $\sqrt{\overline{u_i'u_i'}}\ \sqrt{\overline{v_i'v_i'}}$. Note that it may obtain this value only if the fluid and particle velocities are perfectly correlated. Considering this most extreme case the particles will be a source of kinetic energy to the turbulence if $\overline{v_i'v_i'}$ is greater than $\overline{u_i'u_i'}$. This is not possible because Eq. (16) shows that the energy of a particle at frequency ω is less than the fluid energy at the same frequency by the factor $1 + \omega^2\tau_p^2$. The integration of $E_p(\omega)$ yields the mean-square particle kinetic energy and therefore $\overline{v_i'v_i'}$ is less than $\overline{u_i'u_i'}$. Thus the effect of the particles is to act as an additional source of dissipation of the turbulence kinetic energy.

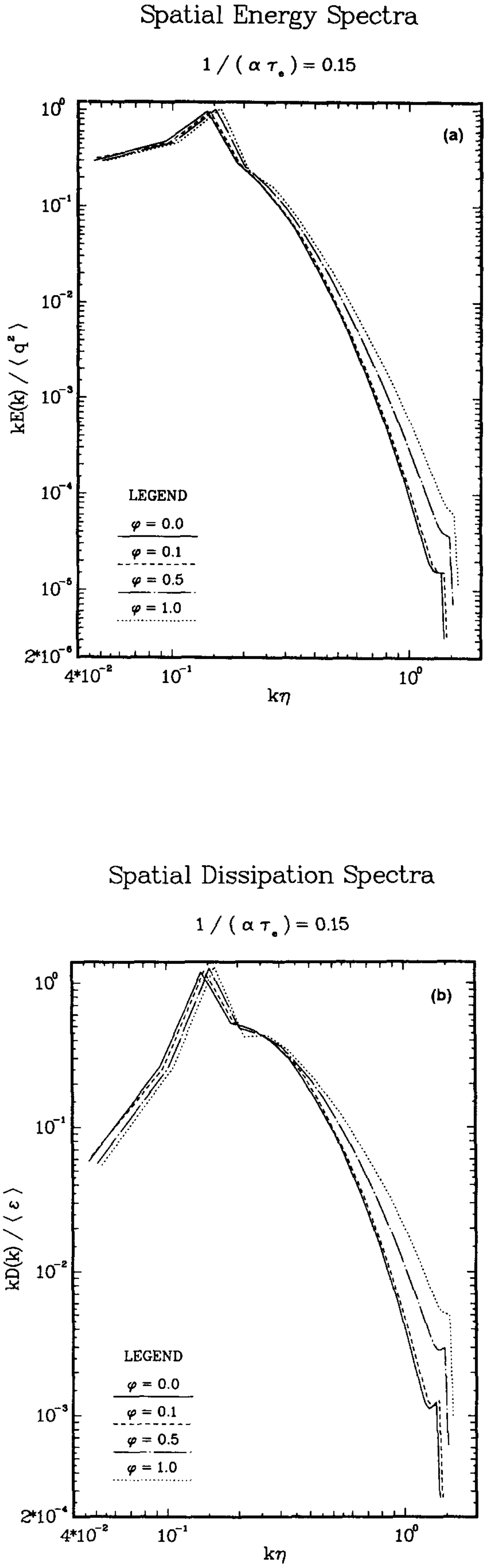

FIG. 7. Effect of loading on spatial spectra from 64^3 simulations, $\tau_p/\tau_e = 0.15$. (a) The spatial energy spectra; (b) the spatial dissipation spectra.

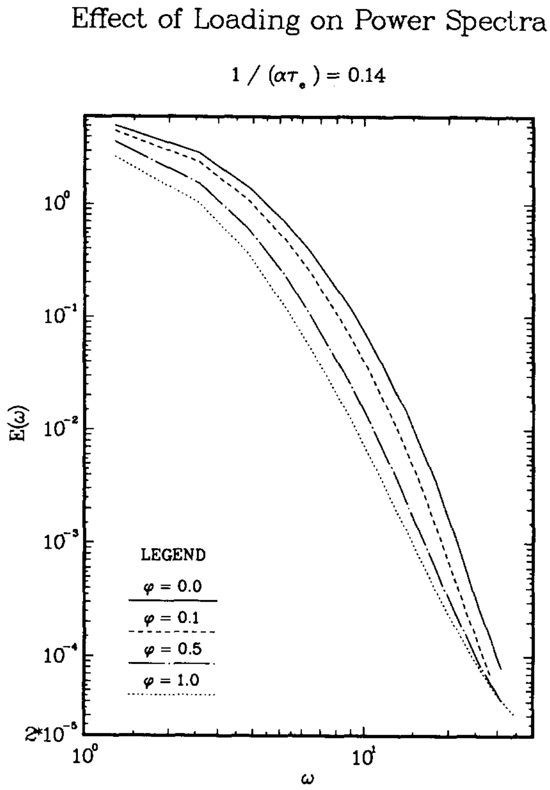

FIG. 8. Effect of loading on frequency spectra from 32^3 simulations, $\tau_p/\tau_e = 0.14$.

Spatial energy spectra for $\tau_p/\tau_e = 0.15$ are shown in Fig. 7(a) for each of the mass loadings used in the simulations. This figure shows that as the mass loading is increased the distribution of energy at the high wave numbers increases relative to the energy in the low modes. The spatial dissipation spectra are shown in Fig. 7(b) and it may also be seen from this figure that the dissipation at the high wave numbers is increased relative to the low wave numbers for increased loading. This increase of the distribution of energy at the high wave numbers relative to that in the low modes was found for all particle time constants used in the simulations.

The effect of loading on the power spectra of the turbulence is shown in Fig. 8. The spectra in Fig. 8 are from the 32^3 simulations for particles with $\tau_p/\tau_e = 0.14$. These spectra are shown as opposed to spectra from the 64^3 simulations since a longer time series was available from the 32^3 simulations. This figure shows that as the mass loading is increased the energy at a given frequency is decreased, consistent with the result that the turbulence kinetic energy is decreased for increasing mass loadings. It is also evident from Fig. 8 that there is not a selective modification of the turbulence in any frequency band. None of the loadings or any of the particle time constants used in the simulations showed a selective modification of the spectrum. It might be expected that for high Reynolds number turbulence, where there is a large range of scales, selective attenuation within specific frequency bands may occur.

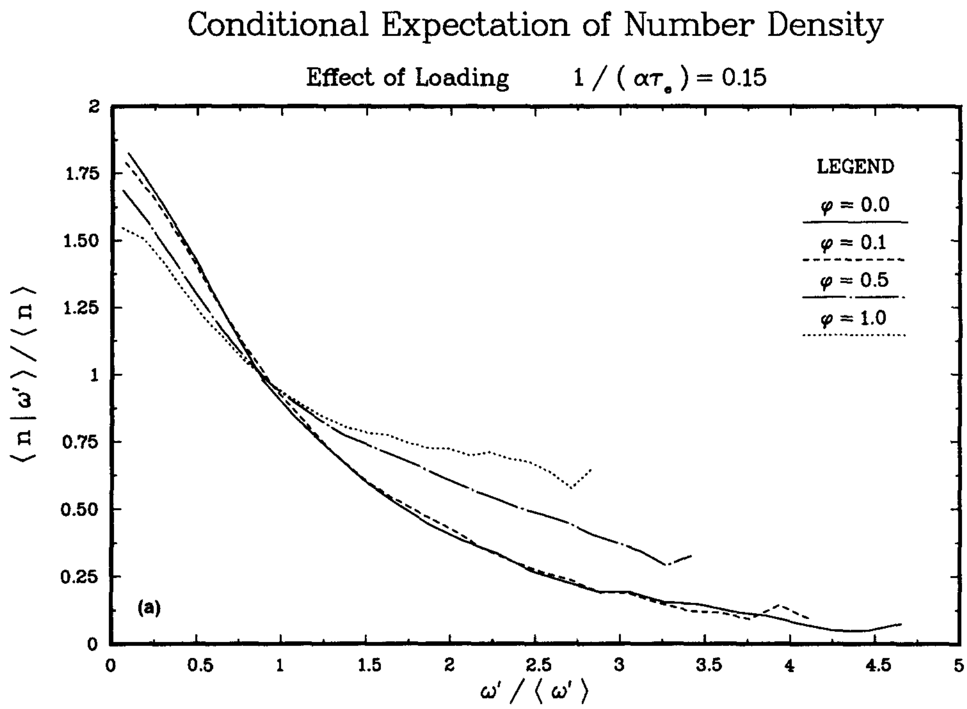

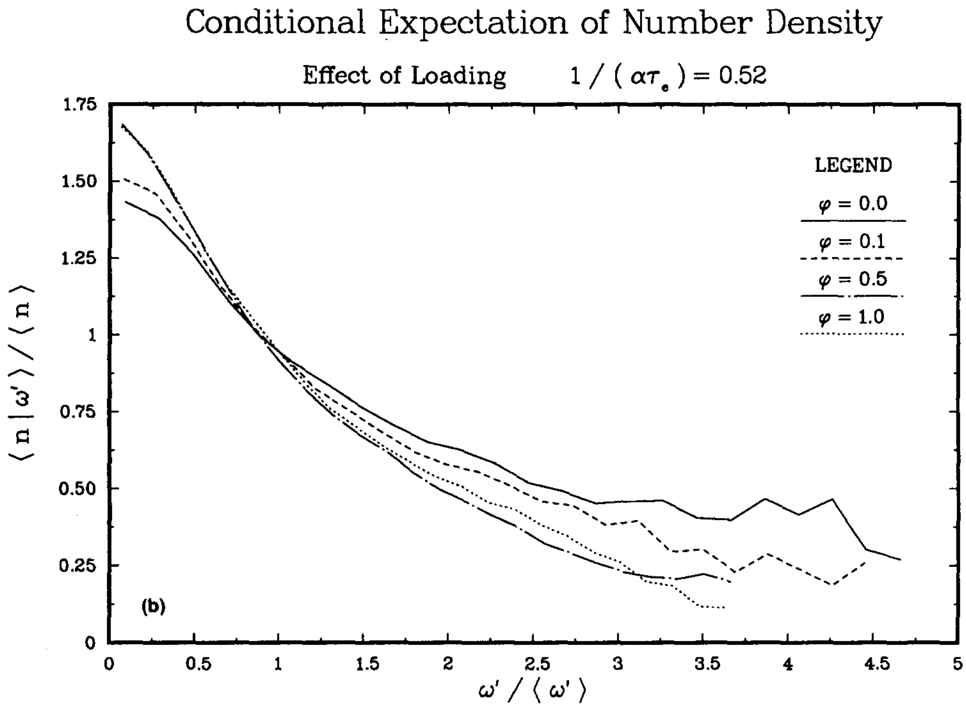

FIG. 9. Effect of loading on the conditional expectation of the number density given the vorticity magnitude from 64^3 simulations. (a) $\tau_p\tau_e = 0.15$; (b) $\tau_p/\tau_e = 0.52$.

Thus one possible reason selective modification does not occur could be due to the low Reynolds numbers of these simulations.

D. Effect of loading on number density field

The effect of mass loading on the conditional expectation of the number density given the magnitude of the vorticity is shown in Fig. 9(a) for $\tau_p/\tau_e = 0.15$. As can be seen from the figure, increased coupling between the phases reduces the tendency for particles to collect in regions of low vorticity. The same quantity is shown in Fig. 9(b) for $\tau_p/\tau_e = 0.52$ and the opposite behavior is observed, i.e., the expectation of the number density is increased for larger mass loadings at low values of the vorticity. This finding is also in agreement with results from the 32^3 simulations. The conditional expectation of the number density given II_d for $\tau_p/\tau_e = 0.15$ and $\tau_p/\tau_e = 0.52$ are shown in Figs. 10(a) and 10(b), respectively. The expectation of the

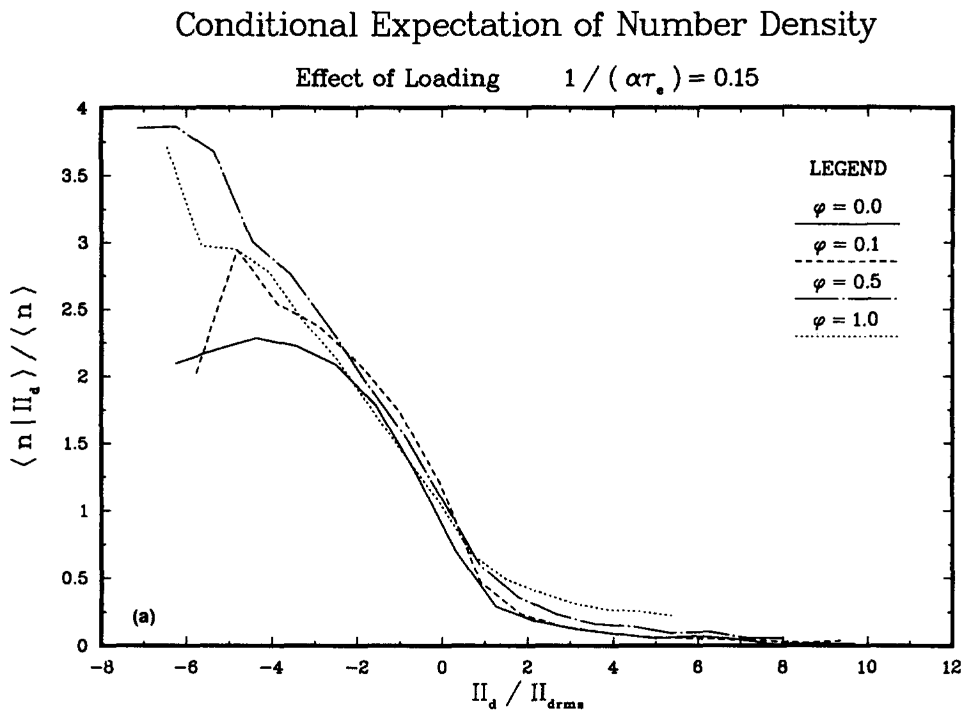

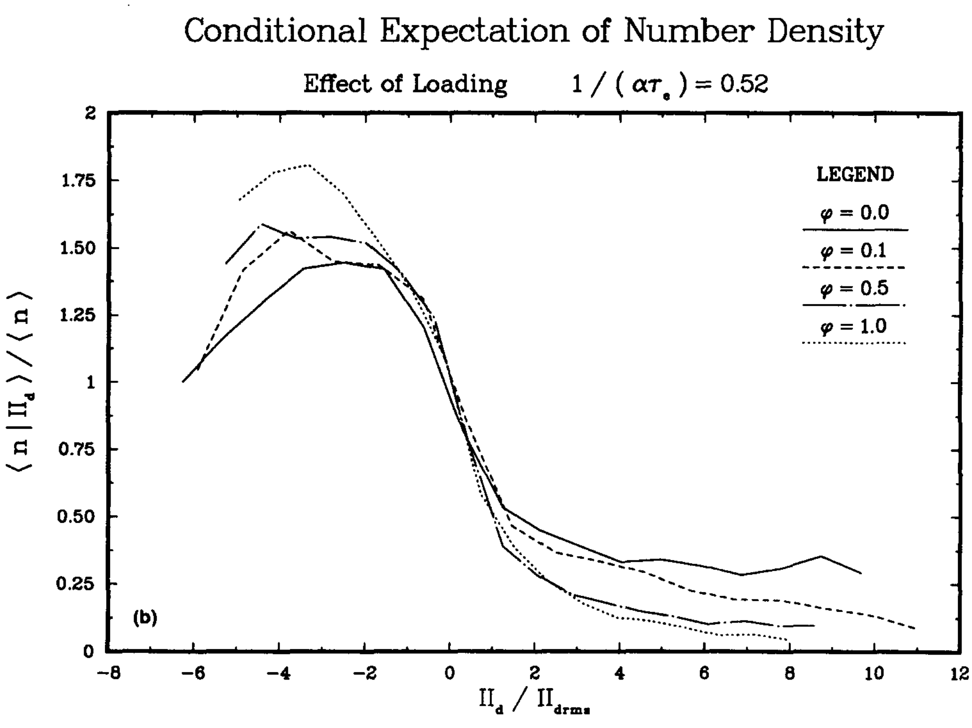

FIG. 10. Effect of loading on the conditional expectation of the number density given the second invariant of the deformation tensor from 64^3 simulations. (a) $\tau_p \tau_e = 0.15$; (b) $\tau_p/\tau_e = 0.52$.

TABLE IV. Effect of loading on correlations between number density and enstrophy and number density and II_d for 64^3 simulations.

ϕ	$\tau_p/\tau_e = 0.15$ $\overline{nce}$	$\overline{ncII_d}$	$\tau_p/\tau_e = 0.52$ $\overline{nce}$	$\overline{ncII_d}$
0.0	− 0.183	− 0.249	− 0.148	− 0.200
0.1	− 0.188	− 0.260	− 0.166	− 0.206
0.5	− 0.154	− 0.269	− 0.193	− 0.230
1.0	− 0.117	− 0.259	− 0.187	− 0.230

number density exhibits the same behavior as shown in Figs. 9(a) and 9(b) for regions where the second invariant is large and positive. However, both figures show that as the mass loading is increased the particles show an increased tendency to be found in regions of high strain rate.

The correlation coefficients between number density and enstrophy and number density and II_d are shown in Tables IV and V. The values in these tables assist in quantifying the effects seen in Figs. 9(a), 9(b), 10(a), and

TABLE V. Effect of loading on correlations between number density and enstrophy and number density and II_d for 32^3 simulations.

ϕ	$\tau_p/\tau_e = 0.14$ $\overline{nce}$	$\overline{ncII_d}$	$\tau_p/\tau_e = 0.75$ $\overline{nce}$	$\overline{ncII_d}$	$\tau_p/\tau_e = 1.50$ $\overline{nce}$	$\overline{ncII_d}$
0.0	−0.168	−0.240	−0.144	−0.219	−0.113	−0.151
0.1	−0.149	−0.272	−0.176	−0.231	−0.104	−0.151
0.5	−0.071	−0.289	−0.183	−0.287	−0.142	−0.211
1.0	−0.063	−0.290	−0.215	−0.286	−0.237	−0.266

10(b). For the lightest particles used in the 32^3 and 64^3 simulations the correlation between number density and enstrophy is decreased by increased mass loading, whereas this correlation is increased for the heavier particles used in the simulations as the mass loading increases. The correlation coefficients between number density and II_d increase as the mass loading is increased for all particle time constants used in the simulations. Since the correlation between number density and enstrophy decreased with increasing loading for the lighter particles the correlation between the number density and the strain rate must be increasing. The results in Tables IV and V also show that the correlation between number density and II_d exhibits a greater increase with larger mass loadings as the particle time constant increases.

E. Effect of loading on turbulence correlations

The correlation coefficient between enstrophy and pressure, as well as II_d and pressure, are shown in Tables VI and VII for the 32^3 and 64^3 simulations. For the lightest particles used in the simulations the value of the correlation between II_d and pressure decreases slightly with increased mass loading while this correlation is relatively insensitive to increased loading for the heavier particles, showing a small increase in this quantity. The correlation between enstrophy and pressure is also somewhat insensitive to increased mass loading for the heavier particles used in the simulations. Since the heavier particles are more uniformly dispersed throughout the domain the modification of the turbulence field is also more uniform and this perhaps explains why these correlations are not affected by the presence of the dispersed phase.

For the lightest particles used in the simulations the correlation between enstrophy and pressure decreases for increased mass loading. Since vortical regions are associated with regions of low pressure the light particles cause more distortion of these eddies than do the heavy particles. The fact that the correlation between II_d and pressure does not decrease as much for the light particles indicates the possibility of a compensating effect where the high-strain–high-pressure regions are reinforced while the high-vorticity–low-pressure regions are weakened.

TABLE VI. Effect of loading on correlations between enstrophy and pressure and II_d and pressure for 64^3 simulations.

ϕ	$\tau_p/\tau_e = 0.15$ $\overline{ep}$	$\overline{II_d p}$	$\tau_p/\tau_e = 0.52$ $\overline{ep}$	$\overline{II_d p}$
0.0	−0.554	−0.644	−0.554	−0.644
0.1	−0.544	−0.643	−0.571	−0.642
0.5	−0.477	−0.621	−0.568	−0.651
1.0	−0.412	−0.588	−0.550	−0.648

IV. SUMMARY AND CONCLUSIONS

Results of simulations of forced isotropic turbulence performed for zero loading show significant effects of turbulence "structure" on the resulting particle number density field. In agreement with the analysis of Maxey,[16] it was found that for intermediate values of the particle time constant lighter particles showed a strong preference to collect in regions of low vorticity and high strain rate. Extremely light particles exhibit less of a preferential concentration since these particles behave more as fluid elements while extremely heavy particle also do not exhibit a preferential concentration field because they are relatively insensitive to the turbulent velocity fluctuations.

For simulations using a nonzero loading time histories of the turbulence energy and dissipation rate exhibit an adjustment period once the phases are coupled. This adjustment period was found to be between two and three eddy turnover times and was also slightly longer for larger mass loadings. It was also found that the energy and dissipation spectra were increased at the high wave numbers relative to the low modes for larger mass loadings.

Turbulence modification by the light particles was different than the modification caused by the heavy particles. While increased mass loading decreased the tendency for light particles to collect in regions of low vorticity, the number density of heavy particles was greater in regions of low vorticity as the mass loading was increased.

Correlations between quantities such as number density and enstrophy as well as enstrophy and pressure showed that the lighter particles caused a more selective modification of the turbulence properties than did the heavier particles. Correlations between enstrophy and pressure decreased with increased mass loading for the lighter particles used in the simulations. These correlations were relatively insensitive to mass loading for the heavier particles. This would indicate that the heavier particles, which are more uniformly dispersed by the turbulence, cause a more homogeneous modification of the turbulence properties than do the lighter particles.

TABLE VII. Effect of loading on correlations between enstrophy and pressure and II_d and pressure for 32^3 simulations.

ϕ	$\tau_p/\tau_e = 0.14$ $\overline{ep}$	$\overline{II_dP}$	$\tau_p/\tau_e = 0.75$ $\overline{ep}$	$\overline{II_dP}$	$\tau_p/\tau_e = 1.50$ $\overline{ep}$	$\overline{II_dp}$
0.0	−0.525	−0.663	−0.525	−0.663	−0.525	−0.663
0.1	−0.440	−0.685	−0.519	−0.673	−0.463	−0.666
0.5	−0.344	−0.634	−0.479	−0.689	−0.435	−0.658
1.0	−0.271	−0.612	−0.526	−0.693	−0.496	−0.700

ACKNOWLEDGMENTS

The authors are grateful for the assistance provided by Dr. Robert Rogallo at the NASA–Ames Research Center in using his code and Dr. Alan Wray at the NASA–Ames Research Center for his help with the VECTORAL compiler.

This work was supported by the National Science Foundation (Grant No. MEA-83-51417), the Office of Naval Research, and the NASA/Stanford Center for Turbulence Research.

[1] C. T. Crowe, J. Fluid Eng. **104**, 297 (1982).
[2] G. I. Taylor, Proc. London Math. Soc., A, **20**, 196 (1921).
[3] S. Corrsin, in *Mechanique de la Turbulence*, Colloques Internationaux du Centre National de la Recherche Scientifique, No. 108 (C.N.R.S., Paris, 1961), pp. 27–52.
[4] W. H. Snyder and J. L. Lumley, J. Fluid Mech. **48**, 41 (1971).
[5] M. R. Wells and D. E. Stock, J. Fluid Mech. **136**, 31 (1983).
[6] S. E. Elghobashi and G. C. Truesdell, *Direct Simulation of Particle Dispersion in a Decaying Grid Turbulence*, Presented at the 7th Symposium on Turbulent Shear Flows, Stanford University, August 1989.
[7] J. Fung and R. J. Perkins, in *Proceedings of the 2nd European Turbulence Conference* (Springer, New York, 1989).
[8] J. B. McLaughlin, Phys. Fluids A **1**, 1211 (1989).
[9] K. D. Squires and J. K. Eaton, Phys. Fluids A (in press).
[10] K. D. Squires and J. K. Eaton, submitted to J. Fluid Mech.
[11] P. K. Yeung and S. B. Pope, J. Fluid Mech. **207**, 531 (1989).
[12] H. Kobayashi, S. M. Masutani, S. Azuhata, N. Arashi, and Y. Hishinuma, in *Transport Phenomena in Turbulent Flows*, edited by M. Hirata and N. Kasagi (Hemisphere, New York, 1988), pp. 433–466.
[13] N. Kamulu, L. Tang, T. R. Troutt, J. N. Chung, and C. T. Crowe, in *International Conference on Mechanics of Two-Phase Flows*, Taipei, Taiwan, 1989, pp. 199–202.
[14] B. J. Lazaro and J. C. Lasheras, Phys. Fluids A **1**, 1035 (1989).
[15] E. K. Longmire and J. K. Eaton, in *Proceedings of the Korea–U. S. Fluids Engineering Seminar* (Korea Institute of Technology, Taejon, Korea, 1989), pp. 435–454.
[16] M. R. Maxey, J. Fluid Mech. **174**, 441 (1987).
[17] R. Chein and J. N. Chung, Int. J. Multiphase Flow **13**, 785 (1987).
[18] K. D. Squires and J. K. Eaton, in *Turbulence Modification in Dispersed Multiphase Flows*, edited by S. Michaelides and D. Stock (ASME–FED, New York, 1989), Vol. 80, pp. 37–44.
[19] R. A. Gore and C. T. Crowe, in Ref. 18, pp. 31–35.
[20] S. L. Lee and F. Durst, Int. J. Multiphase Flow **8**, 125 (1982).
[21] G. Arnason and D. E. Stock, ASME–FED **10**, 25 (1984).
[22] Y. Tsuji and Y. Morikawa, J. Fluid Mech. **120**, 385 (1982).
[23] C. B. Rogers and J. K. Eaton, Department of Mechanical Engineering Report No. MD-52, Stanford University, Stanford, CA, 1989.
[24] L. Tang, C. T. Crowe, J. N. Chung, and T. R. Troutt, in *International Conference on Mechanics of Two-Phase Flows*, Taipei, Taiwan, 1989, pp. 387–391.
[25] M. R. Maxey and J. J. Riley, Phys. Fluids **26**, 883 (1983).
[26] R. S. Rogallo, NASA Tech. Memo 81315, 1981.
[27] D. Gottlieb and S. A. Orszag, *Numerical Analysis Spectral Methods: Theory and Applications*, CBMS–NSF Regional Conference Series in Applied Mathematics (SIAM, Philadelphia, PA, 1977), Vol. 26.
[28] M. J. Lee and W. C. Reynolds, Department of Mechanical Engineering Report No. TF-24, Stanford University, Stanford, CA, 1984.
[29] J. C. R. Hunt, J. C. Buell, and A. A. Wray, *Proceedings of the 1987 Summer Program*, Report No. CTR-S87, Stanford University, Stanford, CA, 1987.
[30] J. O. Hinze, *Turbulence* (McGraw-Hill, New York, 1975).